EPiC Series in Engineering

Volume 3, 2018, Pages 2441–2448

HIC 2018. 13th International Conference on Hydroinformatics

A Novel Slope Failure Operator for a Non-equilibrium Sediment Transport Model

Jiaheng Zhao[1], Ilhan Özgen[12], Dongfang Liang[3], and Reinhard Hinkelmann[1]

[1] Chair of Water Resources Management and Modeling of Hydrosystems, Technische Universität Berlin, Germany
jiaheng.zhao@wahyd.tu-berlin.de, ilhan.oezgen@wahyd.tu-berlin.de, reinhard.hinkelmann@wahyd.tu-berlin.de

[2] Computational Disaster Mitigation and Reduction Research Unit, RIKEN Advanced Institute for Computational Science, Kobe, Japan

[3] Department of Engineering, University of Cambridge, Cambridge, UK
dl359@cam.ac.uk

Abstract

Complex transport mechanism and interaction between fluid and sediment make the mathematical and numerical modeling of sediment transport very challenging. Different types of models can lead to different results. This paper investigates a non-equilibrium sediment transport model based on the total load. In this type of model, it is assumed that a bed slide will occur if the bed slope reaches a critical angle. This is enabled by means of a slope failure operator. Existing slope failure operators usually suffer from the high computational cost and may fail at wet/dry interfaces. The main contribution of this work is the development of a novel slope failure operator for the total load transport model, based on a modified mass balance approach. The proposed approach is verified in three test cases, involving bank failure, dyke overtopping and a two-dimensional bank failure. It is shown that the proposed approach yields good agreement with analytical results and measurement data.

Keywords: Shallow water, Sediment transport, Total load, Slope failure, Overtopping

1 Introduction

Sediment transport in the flow is responsible for the erosion and deposition processes. Several approaches to model sediment transport and morphodynamics exist. In this work, a total load transport model, which considers both bedload and suspended load transport, is presented. In this type of models, if the slope angle of a noncohesive bed becomes larger than a certain critical value, bed slide or avalanche will occur to achieve a new slope approximately equal to the critical angle [6]. Several operators have been proposed to handle slope failure, cf. e.g. [16, 13]. These operators mainly focus on the mass balance and dual mesh approaches. The main idea of the mass balance approach is to calculate the slope in each cell. If the critical slope is exceeded, then update the bed elevation in a suitable way such that the slope equals to

G. La Loggia, G. Freni, V. Puleo and M. De Marchis (eds.), HIC 2018 (EPiC Series in Engineering, vol. 3), pp. 2441–2448

the critical slope. Here, once the bed elevation of the cell is updated, it is necessary to check its neighborhood to ensure that the modification does not cause another slope to exceed the critical slope. This procedure is repeated until a global stability is reached. In the dual mesh approach, a second mesh is constructed around cell nodes that stores only the bed elevation values. Using this second mesh, slopes are calculated in each cell and bed elevations are updated on this mesh. In this approach, bed elevations are only defined at cell vertices. This approach comes with additional computational cost and difficulties in treating wet/dry fronts. In the present work, a mass balance approach-based novel slope failure operator is derived to obtain an algorithm that is efficient, robust and accurate. The key difference is that no iteration is needed for calculating the mass balance based on this operator. Instead of simply updating the bed elevation in the cell under consideration, the mass difference due to bed elevation change is distributed among neighbor cells.

2 Numerical model

2.1 Hydrodynamic model

Due to the interaction between water flow and river bed, the topography of the river undergoes continuous morphological changes. In this work, the 2D shallow water-sediment equations are used to describe the mass and momentum exchanges between sediment-water mixture flow and bed ([11],[2],[18]). The vertical acceleration is regarded to be negligible, and the pressure is hydrostatic. Considering the influence of sediment movement, additional terms are added to represent the effect of the density change and bed level variation.

$$\frac{\partial h}{\partial t}+\frac{\partial (hu)}{\partial x}+\frac{\partial (hv)}{\partial y}=-\frac{\partial Z_b}{\partial t} \tag{1}$$

$$\begin{aligned}\frac{\partial (hu)}{\partial t}+\frac{\partial (hu^2+\frac{1}{2}gh^2)}{\partial x}+\frac{\partial (huv)}{\partial y}&=gh(S_{bx}+S_{fx})-\frac{\rho_s-\rho_w}{2\rho_m}gh^2\frac{\partial c}{\partial x}\\&\quad+\frac{\rho_s-\rho_w}{\rho_m}\frac{u\partial Z_b}{\partial t}\xi(1-p-c)\end{aligned} \tag{2}$$

$$\begin{aligned}\frac{\partial (hv)}{\partial t}+\frac{\partial (huv)}{\partial x}+\frac{\partial (hv^2+\frac{1}{2}gh^2)}{\partial y}&=gh(S_{by}+S_{fy})-\frac{\rho_s-\rho_w}{2\rho_m}gh^2\frac{\partial c}{\partial y}\\&\quad+\frac{\rho_s-\rho_w}{\rho_m}\frac{v\partial Z_b}{\partial t}\xi(1-p-c),\end{aligned} \tag{3}$$

where, t, x and y are the time and two dimensional Cartesian coordinates respectively, h is the water depth and u and v are the velocity along $x-$ and $y-$ direction, respectively. (S_{bx}, S_{by}) and (S_{fx}, S_{fy}) are the bed slope and friction source term, $S_{bx}=-\partial Z_b/\partial x$, $S_{by}=-\partial Z_b/\partial y$, $S_{fx}=C_f u\sqrt{u^2+v^2}$, $S_{fy}=C_f v\sqrt{u^2+v^2}$, C_f is the bed roughness coefficient determined by the Manning coefficient n and h in the form of $n^2/h^{4/3}$, g represents the gravity acceleration, $\partial Z/\partial t$ represents the rate of the bed elevation change, $\xi=\alpha/\beta+(1-\alpha)$ is the sediment-to-flow velocity coefficient for total sediment transport, α is the sediment transport mode parameter in the range of 0 to 1 which specifies the ratio between the bed load and suspended load, β is the velocity of bed load movement relative to the fluid, values for α and β can be obtained from [5], p is the porosity of bed material. The last two terms on the right hand sides in Eqs. (2), (3) account for the spatial variations in sediment concentration and the momentum transfer between flow and erodible bed because of the sediment exchange and velocity difference between

flow and bed.

$$\rho_m = \rho_s c + \rho_w(1-c) \tag{4}$$

in which, c is the depth-averaged volume concentration; ρ_m is the depth-averaged density of sediment water mixture, ρ_w and ρ_s are the density of water and sediment, respectively.

2.2 Morphodynamic model

The bed elevation is updated as

$$\frac{\partial Z}{\partial t} = [\alpha \frac{q_b - q_{b*}}{L} + (1-\alpha)(D-E)]/(1-p), \tag{5}$$

and the sediment concentration is calculated by,

$$\frac{\partial hc}{\partial t} + \xi \frac{\partial huc}{\partial x} + \xi \frac{\partial hvc}{\partial y} = -\frac{\partial Z}{\partial t}(1-p) \tag{6}$$

where D and E are the deposition and entertainment fluxes representing the settling and entrainment of sediment respectively due to the suspended load transport. q_b is the bed load sediment transport rate (m^2/s); q_{b*} is the bed load transport capacity (m^2/s). Based on the non-equilibrium assumption, L is the adaptation length of sediment transport, which is a characteristic distance for sediment to evolve from non-equilibrium transport into equilibrium transport whose calculation can be found in Wu [17]. The suspended load transport coefficients D and E are calculated by using the equation from Van Rijn [15]. The bed load transport capacity q_{b*} is calculated by Meyer-Peter and Müller [10].

2.3 Numerical approach

The full system of Eqs. (1), (2), (3) and (6) is solved on a triangular mesh. The monotone upstream-centered scheme for conservation laws (MUSCL) scheme from [20] is used to modify the original Godunov discretization [4] to have the second-order accuracy, and a Harten, Lax, and van Leer Riemann solver with the contact wave restored (HLLC) [14] is used for solving the Riemann problem at the cell interfaces. The variables in a cell are updated using the two-stage explicit Runge-Kutta scheme [8, 9, 7]. Friction source term S_f is discretized in a splitting point implicit way [1] to avoid instabilities, the slope source term S_b is calculated based on the slope flux calculation method regarding the density slope from [19], which is added into flux term across the edges. In this work, the Courant-Friedrichs-Lewy condition is followed for maintaining the stability, with CFL = 0.5.
The bottom elevation is updated by integrating Eq. (5) over the cell. The sediment concentration flux is located at the interface is calculated by the contact middle wave. All empirical relationships can be found in Sec. 2.2.

3 Slope failure operator

In the cell-centered finite volume approach, cell-averaged values of the water elevation and bottom elevation are stored at the cell center. At the cell edges, values are reconstructed from the cell-averaged values from the adjacent cells. A different value is reconstructed from the cells located at the left and right hand-side of the edge, which means that the water and bottom elevations at the vertex cannot be unique in a cell-centered finite volume framework. The basic

principle is to conduct a continuity plane for the vertices in the computational cells. In this work, the bottom elevation is only influenced by the integration of the source term like presented in Eq. (5). After updating the bottom elevation, the vertex will be adapted to the new cell averaged bottom elevation, using the mean value of the surrounding cells and corresponding influence area

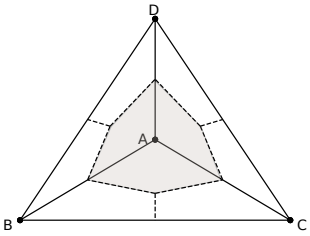

Figure 1: Primary cells surrounding vertex A.

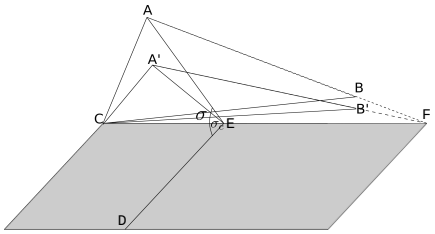

Figure 2: Vertex adjusting for satisfing critical slope.

$$z_v = \frac{\sum(z_i A_i/3)}{\sum(A_i/3)}. \tag{7}$$

Here, z_v and z_i are the bottom elevation of vertex and cell respectively, and i is the index of cell. As shown in Fig. 1, the grey area around vertex A is its influence area, the dashed lines are the lines through the center of gravity and the middle point of edges,

$$\sum_{j=1}^{j=N_v} (z_v^j \sum(A_i/3)) = \sum_{j=1}^{j=N_v} (\sum(z_i A_i/3)), \tag{8}$$

where, j represents the index of vertex, and N_v is the total number of vertices, as every cell has 3 vertices, the right side of Eq. (8) can be changed to $\sum_{i=1}^{i=N_c}(z_i A_i)$, where N_c is the total number of cells. By applying Eq. (7), the cell averaged bottom column will switch to a vertex averaged bottom column. The mass conservation is guaranteed by this approach as shown in Eq. (8). This approach can be extended to unstructured meshes besides triangular meshes.

The angle between horizontal plane and the plane composed by the vertices of the cell can be calculated by mathematical manipulations. If the angle is larger than the critical angle, the following slope failure operator would be used, combined with Fig. 2, the processes are shown as follows:

1. Assume that vertex A is the highest vertex, and C is the lowest one. σ is the angle of the plane ABC and the horizontal plane passes by the lowest vertex C, DEA is the plane perpendicular to the horizontal and ABC plane.

2. Adjust A to A' to satisfy the critical angle σ_c, as the plane is treated as a rotation around line CE, the shape of ABC will stay constant. It can be derived that $z_B/z_A = BF/AF = B'F/A'F = z_{B'}/z_{A'}$, therefore, $z_{B'}$ can be calculated.

3. In order to guarantee the mass balance, the mass loss from vertex A and B will be averaged

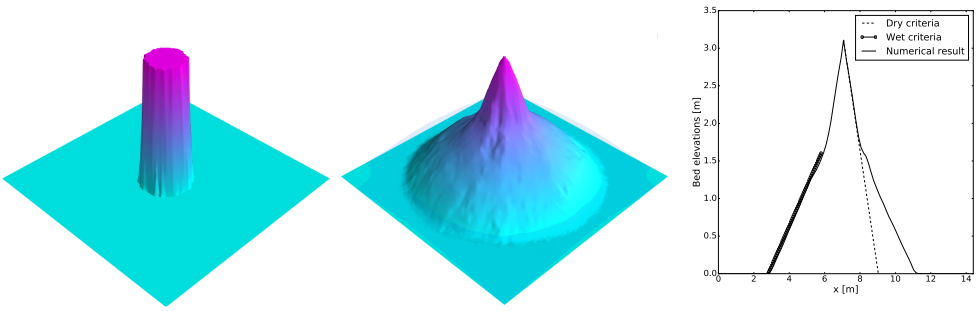

Figure 3: Initial water and bottom elevation(left); final water and bottom elevation(middle); numerical result compared with theoretical critical angle (right).

to the horizontal plane height δz_h,

$$\delta z_h = \frac{(z_A - z_{A'})A_I^A + (z_B - z_{B'})A_I^B}{A_I^A + A_I^B + A_I^C} \tag{9}$$

$$z_A = (z_{A'} - z_C) + \delta z_h,\ z_B = (z_{B'} - z_C) + \delta z_h,\ z_C = z_C + \delta z_h, \tag{10}$$

here, A_I^A, A_I^B, A_I^C are the influence area of vertex A, B, C, respectively.

4. Finally, the bottom elevation of the cell under consideration and the cells adjacent to its vertices are updated using the modified elevation at the vertices.

$$z_i^{new} = z_i + \frac{\delta z_A + \delta z_B + \delta z_C}{3} \tag{11}$$

δz_A, δz_B, δz_C are the difference between the adjusted bottom elevation and the original bottom elevation at vertex A, B, C, respectively.

This slope operator may not yield a final critical slope in each time step, as the adjacent cell will influence the vertex bottom elevation and thus the critical slope will be influenced. In this work, the adjusted treatment will be thought as an approximation to the real physical process.

4 Numerical tests

The proposed slope failure operator is validated in three test cases: one case dealing with bank failure, the second case dealing with overtopping of a dyke [3] and the last test case considering a two-dimensional bank failure in trapezoidal channel [12].

4.1 Ideal bank failure

This test case is set for validating the above algorithm for the slope operator. A sand cylinder with 2 m diameter is set at the middle of a 10 m $\times$ 10 m square domain, part of the cylinder is submerged under the water level (0.5 m) and the critical frication angle for wet and dry sand is 30° and 60°, respectively.

The simulation runs for 10 s until the water level becomes stable, as shown in Fig. 3, the final result can reflect the critical angle properly, but it can be observed that the bottom higher

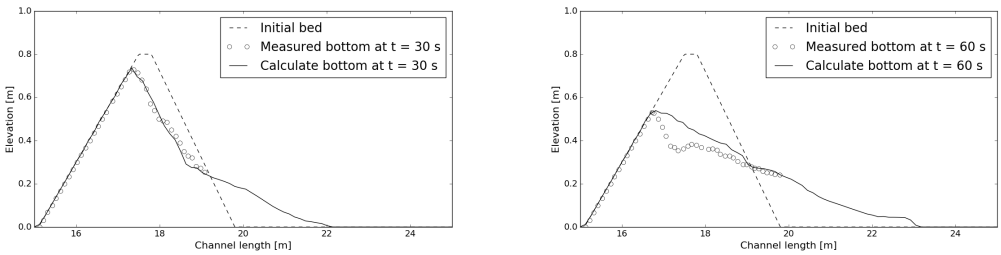

Figure 4: Simulated bed elevation at $t = 30$ s (left) and $t = 60$ s (right).

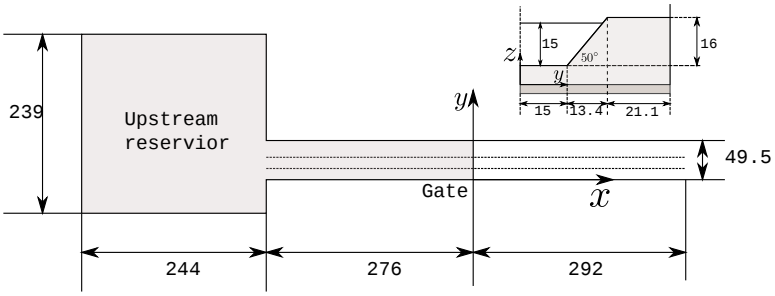

Figure 5: Sketch of dam break through trapezoidal channel: plan view (a), cross section (b) (cm) (after [12]).

than the final water level also obtains a friction angle for wet sand, which is caused by the slip of the bank leading to a wave propagation and the water climbing on the sand cone before the final steady state.

4.2 Dyke erosion due to flow overtopping

Flow overtopping dyke can cause serious erosion and even wash out the structures. Further complex processes involving outburst flow, supercritical flow and steady flow make the sediment movement even more difficult.

The proposed model will be tested against an experiment presented by Chinnarasri *et al.* [3]. The experimental flume is 35 m long and 1 m wide. A 0.8 m high and 1 m wide dyke is located at the middle of the flume, with a crest width of 0.3 m. The upstream and downstream slope of the dyke are set to be 1 : 3 and 1 : 2.5, respectively. The details of the experiment set-up and the parameters can be found in Chinnarasri *et al.* [3]. The friction angle is set to 30°. A comparison of measured and simulated bottom profiles at 30 and 60 s is shown in Fig. 4. The simulated results underestimate a little bit erosion when compared to the measured data at $t = 60$ s, while they agree well with each other at $t = 30$ s.

4.3 Bank failure in a trapezoidal channel

Simulated bed profiles are compared with the laboratory data measured by Soares-Frazão *et al.* [12]. Parameters can be found in [12]. The friction angle for submerged and dry sand are both 37°, and for the humid sand is 87°. As shown in Fig. 6, the bed profiles can be well captured

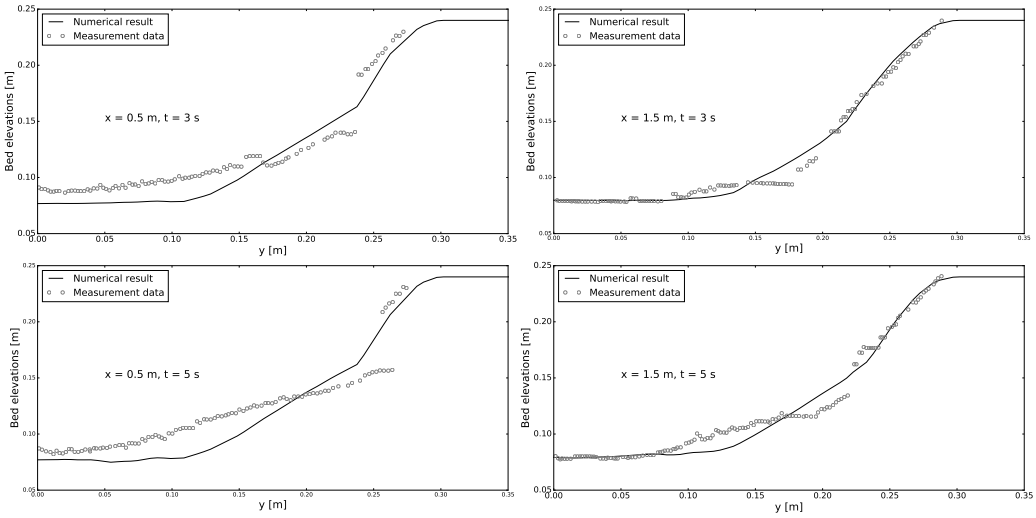

Figure 6: Comparison between numerical results and measurement for bed cross sections at $x = 0.5$, 1.5 m at $t = 3$, 5 s.

for the cross section at $x = 1.5$ m. However, for the cross section at $x = 0.5$ m, the slope is steeper than the measurement, which may be because the overestimated erosion of the main river channel leads to a stable angle closer to the trapezoidal river bank.

5 Conclusions

In this work, a total load transport model with a novel slope failure operator is developed with high efficiency, robustness and accuracy. The proposed operator does not perform additional iterations until global stability is reached, which gives a better computational efficiency. It is suspected, that such iterations are not necessary as the time step in explicit numerical methods is relatively small. The small time steps guarantee an approximately physical slope failure process. Good agreements between model results and measurement data also support this claim, however it will be further investigated in future research.

Acknowledgement

The authors are grateful to the China Scholarship Council and TU Berlin for the scholarships granted to J. Zhao.

References

[1] Thomas RA Bussing and Earll M Murman. Finite-volume method for the calculation of compressible chemically reacting flows. *AIAA journal*, 26(9):1070–1078, 1988.

[2] Zhixian Cao, Gareth Pender, Steve Wallis, and Paul Carling. Computational dam-break hydraulics over erodible sediment bed. *Journal of hydraulic engineering*, 130(7):689–703, 2004.

[3] Chaiyuth Chinnarasri, Tawatchai Tingsanchali, Sutat Weesakul, and Somchai Wongwises. Flow patterns and damage of dike overtopping. *International Journal of Sediment Research*, 18(4):301–309, 2003.

[4] S. K. Godunov. A difference method for numerical calculation of discontinuous equations of hydrodynamics (in Russian). *Matematicheskii Sbornik*, 47:271–300, 1959.

[5] Blair Greimann, Yong Lai, and Jianchun Huang. Two-Dimensional Total Sediment Load Model Equations. *Journal of Hydraulic Engineering*, 134:1142–1146, 2008.

[6] Mingfu Guan, Nigel G Wright, F Asce, and P Andrew Sleigh. Multimode Morphodynamic Model for Sediment-Laden Flows and Geomorphic Impacts. *Journal of Hydraulic Engineering*, 141(6):1–12, 2015.

[7] Jingming Hou, Franz Simons, Mohamed Mahgoub, and Reinhard Hinkelmann. A robust well-balanced model on unstructured grids for shallow water flows with wetting and drying over complex topography. *Computer Methods in Applied Mechanics and Engineering*, 257:126–149, apr 2013.

[8] Qiuhua Liang and Alistair G.L. Borthwick. Adaptive quadtree simulation of shallow flows with wet–dry fronts over complex topography. *Computers & Fluids*, 38(2):221–234, feb 2009.

[9] Qiuhua Liang and Fabien Marche. Numerical resolution of well-balanced shallow water equations with complex source terms. *Advances in Water Resources*, 32(6):873–884, 2009.

[10] Eugen Meyer-Peter and R Müller. Formulas for bed-load transport. In *IAHSR 2nd meeting, Stockholm, appendix 2*. IAHR, 1948.

[11] Guy Simpson and Sébastien Castelltort. Coupled model of surface water flow, sediment transport and morphological evolution. *Computers & Geosciences*, 32(10):1600–1614, dec 2006.

[12] S. Soares-Frazão, N. Le Grelle, B. Spinewine, and Y. Zech. Dam-break induced morphological changes in a channel with uniform sediments: measurements by a laser-sheet imaging technique. *Journal of Hydraulic Research*, 45(July 2015):87–95, 2007.

[13] C. Swartenbroekx, S. Soares-Frazão, R. Staquet, and Y. Zech. Two-dimensional operator for bank failures induced by water-level rise in dam-break flows. *Journal of Hydraulic Research*, 48(3):302–314, 2010.

[14] Eleuterio F. Toro, M. Spruce, and W. Speares. Restoration of the contact surface in the HLL-Riemann solver. *Shock Waves*, 4(1):25–34, jul 1994.

[15] Leo C Van Rijn. Sediment transport, part i: bed load transport. *Journal of Hydraulic Engineering*, 110(10):1431–1456, 1984.

[16] Christian Volz, Patric Rousselot, David Vetsch, and Roland Faeh. Numerical modelling of non-cohesive embankment breach with the dual-mesh approach. *Journal of Hydraulic Research*, 50(6):587–598, 2012.

[17] Weiming Wu. *Computational river dynamics*. Taylor & Francis, 2008.

[18] Junqiang Xia, Binliang Lin, Roger a. Falconer, and Guangqian Wang. Modelling dam-break flows over mobile beds using a 2D coupled approach. *Advances in Water Resources*, 33(2):171–183, 2010.

[19] Jiaheng Zhao, Ilhan Özgen, Dongfang Liang, and Reinhard Hinkelmann. Comparison of depth-averaged concentration and bed load flux sediment transport models of dam-break flow. *Water Science and Engineering*, pages 287–294, 2017.

[20] Jiaheng Zhao, Ilhan Özgen, Dongfang Liang, and Reinhard Hinkelmann. Improved multislope muscl reconstruction on unstructured grid for shallow water equations. *International Journal for Numerical Methods in Fluids*, 2018. fld.4499.